Efficient Statistical Model for Predicting Electromagnetic Wave Distribution in Coupled Enclosures

Shukai Ma[1,*] Sendy Phang[2,3] Zachary Drikas,[4] Bisrat Addissie,[4] Ronald Hong,[4] Valon Blakaj,[2]
Gabriele Gradoni,[2,3] Gregor Tanner,[2] Thomas M. Antonsen,[5,6] Edward Ott,[5,6] and
Steven M. Anlage[1,6]

[1]*Quantum Materials Center, Department of Physics, University of Maryland, College Park, Maryland 20742, USA*
[2]*School of Mathematical Sciences, University of Nottingham, Nottingham NG7 2RD, United Kingdom*
[3]*George Green Institute for Electromagnetics Research, University of Nottingham, Nottingham NG7 2RD,
United Kingdom*
[4]*U.S. Naval Research Laboratory, Washington, DC 20375, USA*
[5]*Department of Physics, University of Maryland, College Park, Maryland 20742, USA*
[6]*Department of Electrical and Computer Engineering, University of Maryland, College Park,
Maryland 20742-3285, USA*

The random coupling model (RCM) has been successfully applied to predicting the statistics of currents and voltages at ports in complex electromagnetic (EM) enclosures operating in the short-wavelength limit. Recent studies have extended the RCM to systems of multimode aperture-coupled enclosures. However, as the size (as measured in wavelengths) of a coupling aperture grows, the coupling matrix used in the RCM increases as well, and the computation becomes more complex and time consuming. A simple power balance (PWB) model can provide fast predictions for the *averaged* power density of waves inside electrically large systems for a wide range of cavity and coupling scenarios. However, the important interference-induced fluctuations of the wave field retained in the RCM are absent in the PWB model. Here we aim to combine the best aspects of each model to create a hybrid treatment and study the EM fields in coupled enclosure systems. The proposed hybrid approach provides both mean and fluctuation information of the EM fields without the full computational complexity of the coupled-cavity RCM. We compare the hybrid model predictions with experiments on linear cascades of over-moded cavities. We find good agreement over a set of different loss parameters and for different coupling strengths between cavities. The range of validity and applicability of the hybrid method are tested and discussed.

I. INTRODUCTION

The ability to characterize and predict the nature of short-wavelength electromagnetic (EM) waves inside interconnected enclosures is of interest to various scientific fields. Applications include EM compatibility studies for electronic components under high-power microwave exposure [1,2], coupled quantum mechanical systems modeled with superconducting microwave billiards [3], cascades of quantum dots [4–7] by way of analogy, and *smart home* sensors in furnished indoor environments. The enclosures in these applications are generally electrically large with an operating wavelength $\lambda \ll V^{1/3}$, where V is the volume of the system. The interior geometry of these enclosures is often complex, including wall features and internal objects

acting as scatterers and geometrical details may not be precisely specified. These systems are then well described as ray-chaotic enclosures, where the trajectories of rays with slightly different initial conditions diverge exponentially with an increasing number of bounces off the irregular walls and interior objects [8–10]. This ray-chaotic property has inspired research in diverse contexts such as acoustic [11–13] and microwave cavities [14–20], the spectral properties of atoms [21] and nuclei [22], and quantum dot systems [23].

Benefiting from the continuing advance in computational capabilities, deterministic approaches utilizing numerical techniques are widely applied in simulating EM quantities inside chaotic systems with specified geometries [24]. The resolution required for deterministic methods, such as the finite difference time domain or the finite element method, scale with the inverse of the wavelength and thus consume a large amount of computational

*skma@umd.edu

resources in the short-wavelength limit (i.e., when typical wavelengths are small compared to the linear scale of the enclosure). In addition, minute changes of the interior structure of a given system will drastically alter the solution of the EM field [19,25]. Statistical methods may thus be more appropriate when studying such systems. Many such approaches have been proposed, examples include the Baum-Liu-Tesche technique [1,26] that analyzes a complex system by studying the traveling waves between its subvolumes, and the power balance (PWB) model [27–30] that predicts the averaged power flow in systems. The PWB method yields predictions of the steady-state averaged energy density inside all system subvolumes based on equating the incoming and outgoing power in each connected subvolume. A version of the PWB method estimating also the variance of the fluctuations has been presented in Ref. [31]. The PWB method is based on the assumption of a uniform field distribution in each cavity that is often fulfilled in the weak intercavity coupling and low damping limit. Extensions of the PWB method that drop the uniform field assumption are ray tracing (RT) methods [32,33] or the dynamical energy analysis (DEA) method [34–36] that calculate local ray or energy densities. DEA and RT capture nonuniformity in the field distribution within a given subvolume. Like the PWB method, they do not treat fluctuations in energy density owing to wave interference.

The random coupling model (RCM) [17,25,37–40] allows for the calculation of the statistical properties of EM fields described in terms of scattering and impedance matrices that relate wave amplitudes, or voltages and currents at ports. The RCM is based on random matrix theory (RMT) originally introduced to describe complex nuclei [22]. It was later conjectured that any system with chaotic dynamics in the classical limit will also have wave properties whose statistics are governed by random matrix theory [41,42]. Here the RCM is applied to wave chaotic systems in the short-wavelength regime. In contrast to the abovementioned methods, the RCM is able to describe the full probability distribution functions (PDFs) for voltages and currents at ports. An exemplary application of the RCM is the simulation of the fluctuating impedance matrix based on minimal system information, namely a single-cavity loss parameter α (to be defined) and several system-specific features [38,39,43–47]. The system-specific features include the radiation information of the ports (both emitting and absorbing), as well as short orbits inside the cavity. The parameter α reflects the loss level of the system, which can be derived from the overall cavity dimension, Q factor, and operating frequency. The RCM has been successfully applied to single cavities and systems of coupled cavities with varying losses, cavity dimensions, and in the presence of nonlinear elements [48,49].

The computational complexity of the RCM grows, however, with the addition of large apertures connecting together multiple enclosures. In the RCM an aperture is treated as a set of M correlated ports, the number of which scales with the area of the aperture as measured in wavelengths squared. For example, a circular shaped aperture whose diameter corresponds to four operating wavelengths allows approximately 100 propagating modes, leading to $M \sim 100$ ports in the RCM modeling of the interconnected cavities. A cavity with M ports is described by an $M \times M$ matrix [37,39,47,50]. When large apertures are present, connecting multiple cavities, the RCM model can become cumbersome. First, there is the need to calculate the matrix elements for each aperture that describe the passage of waves through an aperture radiating into free space. Second, these matrices must be combined with random matrices that give the statistical fluctuations. Third, the RCM is a Monte Carlo method in which the matrices simulating the cavities are constructed for each realization, and many realizations may be required to get accurate statistical results. Finally, the matrices must be connected together, which involves inverting the submatrices representing the subvolumes inside a complex system for each realization [47]. There is thus a need to develop a simple statistical method that applies in cases where the apertures are larger than a wavelength, but small enough so that the two enclosures connected by the aperture can be considered as two separate volumes.

Here, we introduce a hybrid approach that combines the PWB model and RCM to generate statistical predictions of the EM field for multicavity systems without the computational complexity of a full RCM treatment. The hybrid approach is valid in cases where the coupling between adjacent cavities is carried by many channels owing to, for example, large apertures as described above. Using the hybrid method, we apply the PWB method to compute the average EM field intensities in each cavity and use the RCM to predict the fluctuations in the cavity of interest only. The modeling of multiple channels between adjacent cavities is thus reduced to computing a scalar coupling coefficient in the PWB model, often given through simple expressions involving the area of the aperture. A coupled RCM model still needs to be applied where the number of connecting channels between enclosures is small. Such small apertures act as "bottlenecks" for the wave dynamics and a full RCM treatment is necessary to characterize the fluctuations correctly; see also Sec. V and Appendices C and D. From nested reverberation chamber modeling, it is known that weak coupling (bottlenecks) introduces statistical independence of the two cavity environments [51] in the sense that the coupled problem can be described in terms of a random multiplicative process leading to products of random fields. This leads to strong deviations from a Gaussian random field hypothesis, as discussed in more detail in Sec. V and Appendix C. One may further

reduce the computational cost of the hybrid model using a simplified treatment, as proposed in Appendix E. This simplified version of the hybrid model does not require additional knowledge of the frequency-dependent aperture admittance, which is usually obtained through full-wave simulations.

We test the hybrid model using cavity-cascade systems, that is, linear arrays of coupled complex systems. RCM-based studies for a linear multicavity array with a single coupling channel and multiple channels were treated in Refs. [1,17,50]. In the following, we introduce the experimental setup of the cavity cascade system in Sec. II. The formulation of the hybrid PWB-RCM method is presented in Sec. III. In Sec. IV, we compare our model simulations with experimental results. The limits of the hybrid model are studied in Sec. V with conclusions presented in Sec. VI. We relegate technical details to Appendices A–E. These contain an in-depth analysis of the limitations of the hybrid model depending on the number of coupling channels in Appendix C, and extension of the hybrid model including "bottlenecks" in Appendix D, and a simplified version of the original hybrid model in Appendix E.

FIG. 1. A schematic view of the experimental setup. We measure the 2×2 S matrix of a cavity cascade system with a VNA between single-mode ports labeled TX and RX. The cavities are connected through multimode circular apertures from $1 \rightarrow 2 \rightarrow 3$. Rotatable mode stirrers are employed in each cavity to generate different system configurations. The 1- and 2-cavity system measurements are conducted by blocking the apertures and moving the location of the RX port to cavities 1 and 2, respectively.

II. EXPERIMENTAL SETUP

We study the transmission and reflection of EM waves in chaotic multicavity systems. A series of individual cavities is connected into a linear cascade chain through circular-shaped apertures, as shown schematically in Fig. 1. Each cavity is of the same size and shape, but contains a mode stirrer that makes the wave scattering properties of each cavity uniquely different [52]. The total number of connected cavities is varied from 1 to 3. Short-wavelength EM waves from 3.95 to 5.85 GHz are injected into cavities of dimension $0.762 \times 0.762 \times 1.778$ m^3 through WR187 single-mode waveguides, shown as T(R)X in Fig. 1. The loss factor of the system is tuned by placing rf absorber cones inside each cavity. The cavities are large compared with typical wavelengths of the EM field (with $\lambda = 7.49$–5.12 cm and there are approximately 10^4 modes in the frequency range in operation) simulating realistic examples of wave chaotic enclosures. The diameter of the aperture is 0.26 m, and this requires on the order of approximately 100 modes to represent the fields in the aperture at the operating frequency. The thickness of the aperture is about 0.04 times the operating wavelength. We measure the 2×2 scattering (S) matrices of the entire cavity cascade system between ports TX and RX with a vector network analyzer (VNA) from which we deduce the 2×2 impedance (Z) matrix. The S and Z matrices are connected through the bilinear transformation

$$\underline{\underline{S}} = \underline{\underline{Z}}_0^{1/2} (\underline{\underline{Z}} + \underline{\underline{Z}}_0)^{-1} (\underline{\underline{Z}} - \underline{\underline{Z}}_0) \underline{\underline{Z}}_0^{-1/2},$$
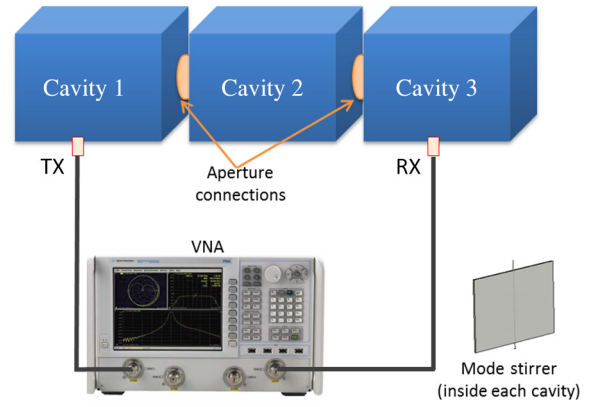
where $\underline{\underline{Z}}_0$ is a diagonal matrix whose elements correspond to the characteristic impedances of the waveguide channels leading to the ports. Independent mode stirrers are employed inside each cavity to create a large ensemble of statistically distinct realizations of the system [53–56]. All mode stirrers are rotated simultaneously to ensure a low correlation between each measurement. A total number of 200 distinct realizations of the cavity cascade are created.

In the RCM, the "lossyness" of a single cavity is characterized by the loss parameter α defined as the ratio of the 3-dB bandwidth of a mode resonance to the mean frequency spacing between the modes [19,45]. The loss parameter α has values larger than 0 (with $\alpha = 0$ corresponding to no loss), where α corresponds roughly to the number of overlapping modes at a given frequency. For the RCM to be valid, there is an upper limit on α determined by the following conditions: (i) the loss rate and mode density should be relatively uniform over the range of frequencies considered and (ii) the number of overlapping modes should be much less than the number of modes used in the RMT construction of the RCM normalized impedance matrix (see Sec. III).

The magnitude of the induced voltage at a load attached to the last cavity in the chain, $|U_L|$, can be calculated from the measured impedance matrix $\underline{\underline{Z}}$ of the cavity cascade system [25]. In the experiment, the load is the RX receiver in the VNA ($Z_L = 1/Y_L = 50\Omega$). Our objective is to use the hybrid PWB-RCM method to describe the statistics of the load voltage $|U_L|$ using a minimum amount of

information about the cavities and minimal computational resources.

III. THE HYBRID MODEL

A. PWB in the hybrid model

The PWB method can be used to determine mean values of EM power flow and energy in systems of coupled cavities [27–30]. For a multienclosure problem, the PWB method solves for the mean power density S_i in each enclosure (i is the cavity index) by balancing the powers entering and leaving each cavity. These power transfer rates are characterized in terms of area cross sections (σ), such that the power transferred is σS_i. Various loss channels, such as aperture-port leakage, cavity wall absorption, and lossy objects inside the enclosure are characterised through the corresponding cross sections σ_o, σ_w, and σ_{obj}, respectively [29]. Constant power is injected into the coupled systems through sources in some or all of the enclosures. The method solves for a steady-state solution when the inputs and losses are made equal for each individual cavity in the system reaching a power balanced state. The PWB method does not contain phase information of the EM fields and thus does not describe fluctuations owing to interference. This can lead to an incomplete prediction of enclosure power flow in the case of small apertures, as discussed in Secs. III C and V B and Appendix C.

B. RCM in the hybrid model

As introduced in Sec. I, the random coupling model provides an alternative method to describe the statistics of the EM fields in a wide variety of complex systems. In contrast with the PWB method, the RCM deals with both the mean and fluctuations of the cavity fields.

For coupled-cavity systems, the RCM multicavity treatment begins with the modeling of the fluctuating impedance matrix of each individual cavity [47]. These matrices relate the voltages and currents at the ports of a cavity. When cavities are connected, the voltages at the connecting ports are made equal and the connecting currents sum to 0. The input port on the first cavity is excited with the known signal. This leads to a linear system of equations that can be solved for all the voltages and currents. This system is resolved for each realization of the cavity impedance matrices.

Model realizations of the fluctuating cavity impedance matrix of an individual cavity are created via a normalized impedance matrix $\underline{\underline{\xi}}_{\mathrm{RCM}}$ derived from a random matrix ensemble [37–39,55]. In terms of the normalized impedance matrix, the fluctuating cavity impedance matrix is written as

$$\underline{\underline{Z}}_{\mathrm{cav}} = i\,\mathrm{Im}[\underline{\underline{Z}}_{\mathrm{avg}}] + \mathrm{Re}[\underline{\underline{Z}}_{\mathrm{avg}}]^{1/2} \cdot \underline{\underline{\xi}}_{\mathrm{RCM}} \cdot \mathrm{Re}[\underline{\underline{Z}}_{\mathrm{avg}}]^{1/2},$$

where the quantity $\underline{\underline{Z}}_{\mathrm{avg}}$ is discussed below. Here, $\underline{\underline{\xi}}_{\mathrm{RCM}}$ is defined as

$$\underline{\underline{\xi}}_{\mathrm{RCM}} = -\frac{i}{\pi} \sum_n \frac{\underline{w}_n\,\underline{w}_n^T}{(k_0^2 - k_n^2)/\Delta k_n^2 + i\alpha},$$

where the sum over n represents a sum over the modes inside the cavity. The vector $\underline{w}_n$, whose number of elements equals the number of ports, consists of independent, zero-mean, unit-variance random Gaussian variables that represent the coupling between each port and the nth cavity mode. This random choice of mode-port coupling originates from the so-called Berry hypothesis, where the cavity modes can be modeled as a superposition of randomly distributed plane waves [57]. The quantities k_0 and k_n are wave numbers corresponding to the operating frequency $\omega_0 = k_0 c$ and the resonant frequencies of the cavity modes, $\omega_n = k_n c$. Rather than use the true resonant frequency of the cavity, a representative set of frequencies is generated from a set of eigenvalues of a random matrix selected from the relevant random matrix theory ensemble [15,37,58,59]. These RMT eigenvalues are appropriately normalized to give the correct spectral density via the parameter Δk_n^2. The loss parameter $\alpha = k^2/(Q\Delta k_n^2)$, where k is the wave vector of interest and Q is the quality factor [45].

System-specific information about the enclosure is captured in the averaged impedance matrix for each cavity, Z_{avg} [43]. Here, the average impedance matrix can be thought of in two ways. First, it can be considered as a window average of the exact fluctuating cavity matrix over a frequency range, ω_2, centered at frequency ω_1. In the case in which the windowing function is Lorenzian this average is equivalent to evaluating the exact cavity matrix at complex frequency $\omega_1 + i\omega_2$. This in turn is the response matrix for exponentially growing signals with real frequency ω_1 and growth rate ω_2. This leads to the second way of understanding the average impedance matrix. It is the early time ($\omega_2 t < 1$) response of the ports of the cavity. Thus, the average impedance matrix can be calculated by assuming that the walls of the cavity have been moved far from each port, and that each port responds as if there were only outgoing waves from the port. In the case of apertures as ports, the transverse electric and magnetic fields in the aperture opening are expanded in a set of basis modes with amplitudes that are treated as port voltages in the case of an electric field, and port currents in the case of a magnetic field. The linear relation between these amplitudes is calculated for the case of radiation into free space, and this becomes the average aperture admittance-impedance matrix. Each mode in the aperture field representation is treated as a separate port in the cavity matrix. Thus, the dimensions of the matrix grows rapidly with the addition of a large aperture [50].

In the cavity cascade system, the abovementioned apertures (with M propagating modes) are adopted as the
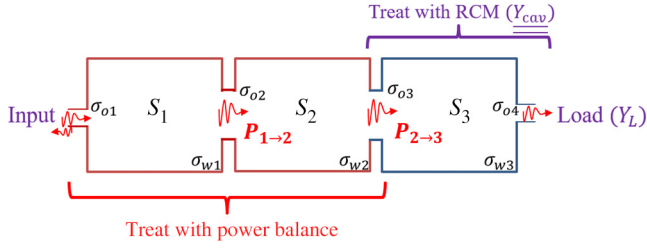
FIG. 2.   Schematic illustration of the hybrid model applied to a 3-cavity cascade. In the hybrid model, we use the PWB method to characterize the power flow from the first cavity to the next to last cavity. The fluctuations in the final cavity are described using the RCM method using the mean power flow values obtained from the PWB method as an input.

connecting channel between neighboring cavities. With M connecting channels between cavities, the dimension of the above-defined cavity impedance matrix becomes $M \times M$. The matrix multiplications and inversions in the calculation of RCM multicavity formulations [47] thus have complexity that grows as $O(M^{2.4})$ using common algorithms [60]. Thus, for large M, the computational cost of the RCM scales roughly as $N \times M^{2.4}$, where N represents the number of cavities in the system.

Here we propose a hybrid method for multicavity problems that combines both the PWB model and RCM, as shown schematically in Fig. 2. In an N-cavity cascade system with multiple channel connections between adjacent cavities, we utilize the PWB method to characterize the mean flow of EM waves from the input port of the first

cavity to the input aperture of the last (Nth) cavity. The RCM method is now applied to the last cavity and the connected load at the single-mode output port of that cavity. Thus, the hybrid method combines the strengths of both methods: the fluctuations of the EM field will be captured with RCM, and the computational cost is greatly reduced using the PWB method. A quantitative comparison of the computational costs between the full RCM method and the hybrid method is discussed later in Sec. III D.

In the following, we discuss the hybrid model formulation in detail based on the 3-cavity system example shown in Fig. 2. We will first introduce the PWB treatment to the first two cavities in the chain, followed by the modeling of the last cavity using the RCM in Sec. III C. We will then discuss how to connect the PWB model and RCM at the aperture plane between the last two cavities in Sec. III D. With the model formulation introduced, we will look into the validity of the hybrid model in Sec. III E. A step-by-step protocol to apply the PWB-RCM fusion to generic cavity systems is detailed in Appendix D.

C. Detailed cavity treatments

The PWB method characterizes the flow of high-frequency EM waves inside a complex interconnected system based on the physical dimensions of the cavities, the cavity quality factors Q, and the coupling cross sections σ_o, as well as the incident power P_{in} driving the system [27,29]. The PWB method then yields the power densities of each individual cavity in steady state. For the 3-cavity cascade system in Fig. 2, the PWB equations are

$$
\begin{bmatrix}
\sigma_{w1} + \sigma_{o1} + \sigma_{o2} & -\sigma_{o2} & 0 \\
-\sigma_{o2} & \sigma_{w2} + \sigma_{o2} + \sigma_{o3} & -\sigma_{o3} \\
0 & -\sigma_{o3} & \sigma_{w3} + \sigma_{o3} + \sigma_{o4}
\end{bmatrix}
\begin{bmatrix}
S_1 \\
S_2 \\
S_3
\end{bmatrix}
=
\begin{bmatrix}
P_{\mathrm{in}} \\
0 \\
0
\end{bmatrix},
\tag{1}
$$

where the σ_{wi}'s refer to the wall loss cross section and S_i is the power density of the ith cavity, σ_{o1} and σ_{o4} are the cross sections of the input and output ports, while σ_{o2} and σ_{o3} represent the aperture cross sections; see Fig. 2. The cross sections can be expressed explicitly from known physical dimensions and cavity wall properties [29]. Here P_{in} is the (assumed steady) incident power flow into the first cavity. In this example, we assume that only the first cavity receives EM power from external sources. The balance between the input and loss is achieved by solving Eq. (1) for the steady-state power densities S_i. For example, the power balance condition of the first enclosure is expressed as $(\sigma_{w1} + \sigma_{o1} + \sigma_{o2})S_1 = P_{\mathrm{in}} + \sigma_{o2}S_2$. The left-hand side of this equation represent the loss channels of the cavity, including the cavity wall loss and the leakage through the

input port and the aperture. The right-hand side describes the power fed into the cavity, consisting of the external incident power and the power flow from the second cavity. The net power that flows into the last cavity in the cascade is expressed as $P_{2 \to 3} = \sigma_{o3}(S_2 - S_3)$.

The last cavity is characterized by the RCM method. With the knowledge of the cavity loss parameter α and the port coupling details, the full cavity admittance matrix of the last cavity can be expressed as [50]

$$
\underline{\underline{Y}}_{\mathrm{cav}} = i \operatorname{Im}(\underline{\underline{Y}}_{\mathrm{rad}}) + \operatorname{Re}(\underline{\underline{Y}}_{\mathrm{rad}})^{0.5} \cdot \underline{\underline{\xi}} \cdot \operatorname{Re}(\underline{\underline{Y}}_{\mathrm{rad}})^{0.5}.
$$

The quantity $\underline{\underline{Y}}_{\mathrm{rad}}$ is a frequency-dependent block-diagonal matrix whose components are the radiation admittance matrices of all the ports and apertures of that cavity. We

assume no direct couplings between apertures because the direct line-of-sight effect is small in the experimental setup. Consider a cavity with two M-mode aperture connections; the dimension of the corresponding matrix $\underline{\underline{Y}}_{\mathrm{rad}}$ is $2M \times 2M$. The matrix elements are complex functions of frequency in general and can be calculated using numerical simulation tools. We use here the software package CST Studio Suite® to calculate the aperture radiation admittance (see Ref. [61] and Appendix B.2 of Ref. [47]). The RCM normalized impedance $\underline{\underline{\xi}}$ is a detail-independent fluctuating "kernel" of the total cavity admittance $\underline{\underline{Y}}_{\mathrm{cav}}$. With known α, an ensemble of the normalized admittance $\underline{\underline{\xi}}$ can be generated through random matrix Monte Carlo approaches [25]. Combining the fluctuating $\underline{\underline{\xi}}$ and $\underline{\underline{Y}}_{\mathrm{rad}}$, an ensemble of "dressed" single-cavity admittance matrices for the final cavity can be generated. It is later shown in Appendix E that a substantial reduction of the hybrid model computational cost is made possible using an aperture-admittance-free treatment, at the price of reduced accuracy for longer cascade chains.

D. The hybrid model

We next connect the PWB and RCM treatments at the interface between the second and third cavities. As discussed in the previous section, the power flow into the third cavity, $P_{2\to3}$, is calculated from the 3-cavity PWB calculation. Identical system setups are utilized in the PWB and RCM treatments, including the operating frequency range, the dimensions of the cavities, ports and apertures, and the loss of the cavity (achieved by a simple analytical relationship between the RCM α parameter and σ_w; see Appendix A for more details). To transfer the scalar power values $P_{2\to3}$ generated by the PWB method into an aperture voltage vector required for the RCM, we assign random voltages $\underline{U}_{o3}$ drawn from a zero-mean, unit-variance Gaussian distribution for the M-mode aperture and calculate the random aperture power using

$$P_{o3} = \frac{1}{2}\mathrm{Re}(\underline{U}_{o3}^* \cdot \underline{\underline{Y}}_{\mathrm{rad}} \cdot \underline{U}_{o3}).$$

These randomly assigned aperture voltages $\underline{U}_{o3}$ are then normalized by the ratio $P_{2\to3}/P_{o3}$ to match with the value calculated from the PWB method. Combined with the RCM-generated cavity admittance matrix $\underline{\underline{Y}}_{\mathrm{cav}}$, an ensemble of induced voltage values U_L at the load on the last cavity is computed utilizing Eq. (C7) of Ref. [47]. The power delivered to the load is obtained using

$$P_L = \frac{1}{2}\mathrm{Re}(U_L^* \cdot Y_L \cdot U_L),$$

where Y_L is the load admittance, taken to be $1/(50\Omega)$ here.

With the formulation of the hybrid model now explained, here we discuss the improvement in computational time and memory usage by replacing the full RCM multi-cavity method with the hybrid model. For an N-cavity system connected through M-mode apertures, the hybrid model requires only a fraction of $1/[(N-1)M^2]$ of the memory consumption as compared to the full RCM method, enabled by the reduced cavity impedance matrix storage for the first $N-1$ cavities. Moreover, the computation time is also reduced by eliminating the RCM modeling of the prior cavities. For example, the computation/CPU time for the two-cavity cascade system with circular aperture connections reduces from about 120s to 40s with application of the hybrid method (tests run on a typical workstation). In addition, the computation time of the full RCM method scales with the total number of cavities in the system N, while the hybrid method is insensitive to the further addition of cavities. Aside from the difference in the CPU time, there is a finite loading time to move the data (e.g. random matrices to model single cavities) from the hard drive to RAM. Compared to the full RCM method, the hybrid model reduces the number of cavities that need RCM modeling from N to 1, and thus decreases the data loading time. The advantage of the method becomes more prominent for larger lengths of the cavity chain N and larger apertures (having M modes).

E. Limits of the hybrid model

The hybrid model is based on the assumption that the fluctuations in a given cavity are independent of the fluctuations in adjacent cavities and thus of the fluctuations in the power flowing between cavities (as a function of frequency, for example). We assess the validity of these assumptions by analyzing a multichannel cascaded cavity system in Appendix C. We study in particular the effect of the total number of effective cavity-cavity coupling channels M_n between the nth and $(n+1)$th cavity on the fluctuation levels of the load-induced power P_L connected to the final cavity. Since $P_L \propto |U_L|^2$, the conclusions drawn from the power-flow studies can also be applied to voltage-related results, as presented below in Sec. IV. Defining the load power fluctuation levels as the ratio $\kappa = \langle P_L \rangle^2 / \langle P_L^2 \rangle$, where $\langle \cdot \rangle$ represents averaging over an ensemble, we treat κ as a measure characterizing the level of fluctuations of the power. Here, $\kappa \sim 1$ and $\kappa \gg 1$ refer to low and high fluctuations of the power values, respectively. In Appendix C, it is shown that

$$\kappa \propto \prod_{n=1}^{N}(1 + M_n^{-1}), \tag{2}$$

where the product is over all the cavities in the cascade. If cavities $n = 1$ to $n = N-1$ have strong multichannel connections owing to, for example, large apertures with

$M_n \gg 1$ propagating modes at the operating frequency, then $M_n^{-1} \to 0$ and the contributions to Eq. (2) not including the coupling to the load, that is, $\prod_{n=1}^{N-1}(1 + M_n^{-1}) \to 1$; this holds for the experiments described in Sec. IV with $M_n \approx 100$ at the frequencies considered. The quantity M_n is small when a single-mode waveguide connects the last cavity (N) to the load (the experiment in Sec. IV). At the last cavity (N) there is a single-mode output port, $M_n = 1$ and the $1 + M_n^{-1} = 2$, which induces higher fluctuations at the load compared to the case where all apertures are large. Similar small M_n situations appear when a "bottleneck" is introduced between cavities (the experiments in Sec. V B). It is therefore sensible to adopt RCM for just the last cavity to capture the power fluctuations at the load, while it is sufficient to include the influence of the intervening cavities with the PWB method only giving the required information about the mean power flow. This case is discussed in Sec. IV. In Sec. V, we also consider the effect of having small aperture connections—referred to as "bottlenecks"—at intermediate locations in the cavity cascade where we see deviations of the hybrid model from a full multicavity RCM treatment.

IV. COMPARISON OF THE HYBRID MODEL WITH EXPERIMENTAL RESULTS AND DISCUSSION

We now conduct the PWB-RCM hybrid analysis for the multicavity experiment and compare with measurements. We consider 2- and 3-cavity cascades with large (on the scale of the wavelength) apertures between the cavities

and single-mode connections to the load in the last cavity. The induced voltages at the load $|U_L|$ are calculated from data using the methods reported in Refs. [25,62], and these experimental results are shown as solid lines in Fig. 3. An ensemble of induced load voltages for the multicavity system is created by moving the mode stirrers in all cavities between each measurement. The losses in the single cavities are altered by inserting equal amounts of rf absorbers in each cavity. In addition, the hybrid PWB-RCM method is used to calculate $|U_L|$ and the resulting distributions are shown as dotted lines in Fig. 3. Good agreement between the measured and model-generated results are observed over a range of different total cavity numbers and single-cavity loss values. Under varying cavity loss conditions, the PDF of the induced load voltage $|U_L|$ of the 3-cavity system has a lower mean value and smaller fluctuations compared to the 2-cavity system results. Going from two to three cavities will decrease the energy density in the last cavity and thus the power delivered to the load. This difference between the 2- and 3-cavity $|U_L|$ becomes smaller when the single-cavity loss decrease, as can be seen following Figs. 3(a)–3(d); see also the inset in Fig. 3(b).

The induced load voltage PDFs of the multicavity system can be generated solely with the RCM formulation [47]. A comparison between the $|U_L|$ PDFs generated with the full RCM method, the hybrid method, and the experiments are shown in Fig. 4. Both theoretical approaches are able to generate statistical ensembles that agree well with the experimental results. We find that the RCM results (dashed lines) slightly outperform the hybrid method
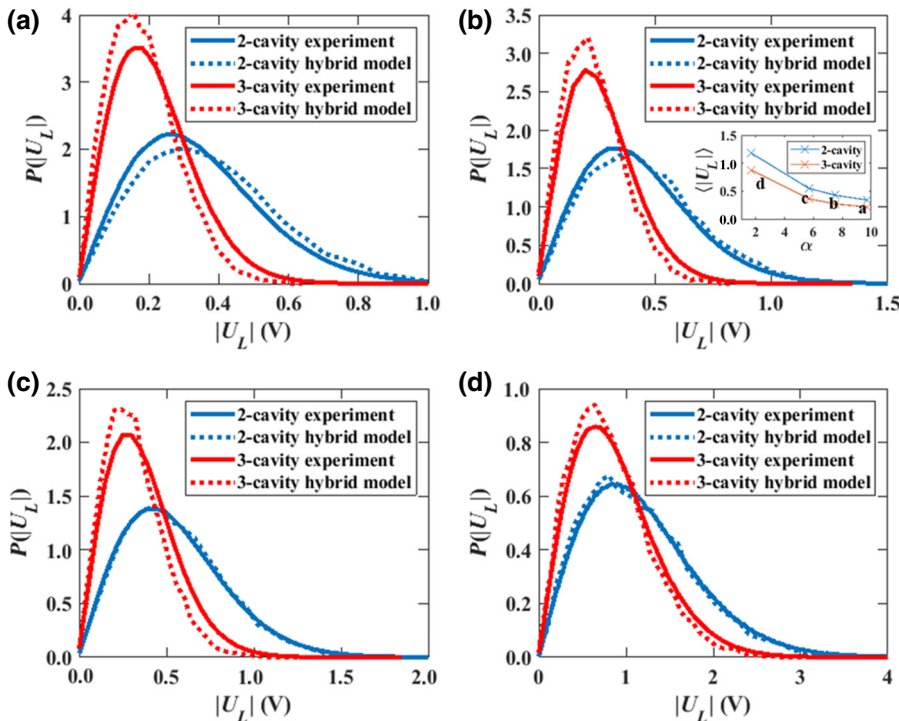

FIG. 3. The PDFs of load-induced voltage $|U_L|$ of 2- and 3-cavity experiments (solid lines) and hybrid model calculations (dashed lines). The single-cavity loss parameter is 9.7, 7.5, 5.7, and 1.7 in (a)–(d), respectively. The inset in (b) shows the 2- and 3-cavity experiment averaged induced voltage values $\langle|U_L|\rangle$ with respect to different loss parameters α. Multimode (approximately 100 modes) circular apertures are employed between the cavities.
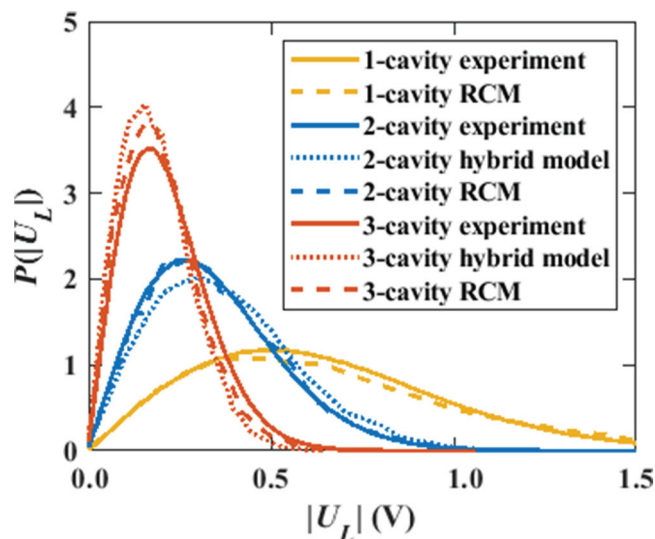
FIG. 4.   Comparison of induced load voltage statistics for the hybrid model (dotted lines), RCM predictions (dashed lines), and experimental results (solid lines) for the case of 2- and 3-cavity cascades with single-cavity loss parameter $\alpha = 9.7$, and circular multimode apertures between the cavities. The frequency range is from 3.95 to 5.85 GHz.

(dotted lines) for the 2-cavity case. However, the computation time and storage cost of the full RCM method is N times larger than the hybrid method, where N refers to the total number of connected cavities in the cascade.

It is well established that the distribution of fields inside sufficiently lossy single or nested cavity systems is Rayleigh or double-Rayleigh distributed [48,51,63,64]. It was shown by the authors of Ref. [48] that the cavity field distribution deviates from a Rayleigh distribution in the low-loss limit ($\alpha < 1$), while the RCM method remains valid. Thus, the RCM method applies to a wider range of complex cavity systems.

V. TESTING THE LIMITS OF THE HYBRID MODEL

As already discussed in Sec. III C, we expect that the hybrid model will break down in the limit where either the RCM and/or PWB methods are no longer valid. We consider two generic types of limitations, namely systems with high loss and systems having "bottlenecks" in the middle of the cavity cascade. These two conditions are experimentally studied using a ×20 scaled down version of the cavity system [19,47]. The dimension of the single miniature cavity is $0.038 \times 0.038 \times 0.089$ m^3. EM waves from 75–110 GHz are fed into the cavity (approximately 10^4 modes at and below the operating frequency range) through single-mode WR10 waveguides from Virginia Diodes VNA extenders and the S parameters are measured by a VNA. We have previously demonstrated that identical

statistical electromagnetic properties are found in this and the full-scale configuration described in Sec. II [47].

A. High and inhomogeneous cavity losses

The proposed hybrid method is not expected to generate accurate predictions for extreme high and inhomogeneous lossy systems [62]. Both PWB and RCM models require uniform power distribution inside the studied system. Such a presumption no longer holds when the loss of the cavity wall becomes so high that the energy distribution near the system boundaries and from the input to output apertures drop considerably. In this case, the PWB model needs to be replaced with other methods, such as ray tracing [33] or the DEA analysis [65], or, in the case of multiple scatterers in each cavity, using an approximate flow solver based on a three-dimensional diffusion model [66]; all these methods have a larger computational overhead compared to the PWB model. Strong damping also violates the random plane wave hypothesis crucial to the RCM [57,62,67]. We experimentally examine the applicability of the hybrid model in the extreme high-loss limit. A 2-cavity cascade system is designed where electrically large (many wavelengths in size) ARC rf absorber panels are placed on a wall inside each cavity. The detailed experimental setup of the extreme high-loss cases can be found in Appendix B. The inclusion of absorber walls creates effectively "openwall" high-loss cavities ($\alpha \sim 25$ for a single cavity) [62]. The measured and the model-generated load-induced voltage statistics are shown in Fig. 5(a) for this case. Neither the hybrid model nor the full RCM model is expected to work in this high and inhomogeneous loss limit. As seen in Fig. 5(a), both models show strong disagreement with the measured data. These inhomogeneities in each cavity are well captured using either ray-tracing or DEA methods, as demonstrated in Ref. [68].

The hybrid model can be applied to the lower-loss systems ($\alpha \sim 1$), as demonstrated in Sec. IV. We point out, however, that the stronger impedance fluctuations of lowloss systems poses greater challenges for the acquisition of good statistical ensemble data for both numerical and experimental methods [64,69].

B. Weak intercavity coupling

Another assumption of the hybrid model is that intermediate cavities have multiple connecting channels; see Sec. III C. We expect that the hybrid model as introduced in Sec. III fails when some or all of the apertures are small, effectively acting as "bottlenecks." The transmission rates then become strongly frequency dependent, thus adding to the overall fluctuations in the system and deviating strongly from the aperture cross sections assumed for the PWB model in Sec. III E. In the experiments, we create a "bottleneck" carrying only five channels between the intermediate
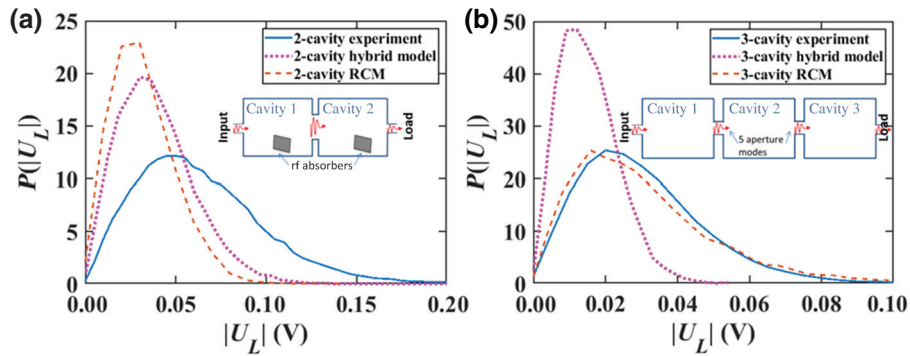
FIG. 5. (a) The load-induced voltage $|U_L|$ statistics $P(|U_L|)$ of the 2-cavity experiment and models in the high loss limit ($\alpha \sim 25$). The cavities are connected with a circular-shaped aperture that supports approximately 100 modes at 110 GHz. The inset shows the experimental setup schematically. (b) The 3-cavity experimental and model-generated load-induced voltage statistics. The cavities ($\alpha \sim 9.1$) are connected by rectangular-shaped apertures with just five propagating modes. The inset shows a schematic of the experimental setup.

cavities of the chain and study how this brings out the limitations of the hybrid model. As discussed in Sec. III E and Appendix C, the fluctuations of the wave flow are then correlated as the energy propagates through the cavity cascade chain; these increased fluctuations of the input power at the last cavity are not captured in a PWB treatment. It is important to point out that the fluctuations of input current at a cavity beyond a bottleneck can no longer be considered Gaussian. The latter aspect is known from cavity systems studied in electromagnetic compatibility; see, for example, the deviation of the received power in a weakly coupled nested reverberation chamber [51]. In Appendix C, arguments are developed to quantify these deviations for cavity cascade systems.

We construct a 3-cavity experiment to test this effect; for more details about the experiment, see Appendix B. The cavities are connected through small rectangular-shaped apertures that allow only five propagating modes as opposed to 100 modes utilized in the experiments discussed earlier; we have $\alpha = 9.1$ for all cavities. In this few-coupling-channel system, the cavities in the cascade have a substantial contribution to the overall fluctuations of neighboring cavities and thus the induced load voltage and power values. As shown in Fig. 5(b), the hybrid model fails to correctly reproduce the statistics of the measured $|U_L|$, while the full RCM cavity cascade formulation retains the ability to correctly characterize the statistics of the system.

To summarize the section, we study the applicability of the hybrid PWB-RCM method to cases where it is expected to fail. It is found that enclosures with large and inhomogeneous losses violate the conditions for the hybrid method. The case of intermediate "bottlenecks" can be handled with the RCM, but not the hybrid model as formulated. A generalization of the hybrid PWB-RCM that can handle arbitrary "bottlenecks" is outlined in Appendix D. The proposed hybrid model is expected to generate statistical mean and fluctuations of the EM fields for systems with moderate cavity losses and large intercavity coupling strengths. Expanding the hybrid model to systems with more complex topology and exploring new types of hybrid models by combining the RCM with other statistical or deterministic methods has been considered in Ref. [70].

VI. CONCLUSION

In this paper, we propose a hybrid PWB-RCM method for the statistical analysis of EM fields in complex, coupled cavity systems based on minimal information of the system. The method is tested and found to be in good agreement with cavity cascade experiments under various conditions, such as varying single-cavity loss and the total number of connected cavities. The limitations of the hybrid model are also discussed and demonstrated experimentally. The hybrid model is computationally low cost and able to describe the statistical fluctuations of the EM fields under appropriate conditions. We believe that the hybrid method may find broad applications in the analysis of coupled electrically large systems with sophisticated connection scenarios.

APPENDIX A: RELATING CAVITY INTERNAL LOSS PARAMETERS IN THE RCM AND PWB MODEL

The parameters used to model the cavity loss in the RCM (α) and PWB model (σ_w) are different. We propose a simple analytical relationship between these internal loss parameters, namely $\alpha = \gamma \sigma_w$. In the RCM, the single-cavity loss parameter α can be written as $\alpha = k^3 V/(2\pi^2 Q)$ for three-dimensional enclosures, where V, Q, and k are the cavity volume, closed cavity quality factor, and the operating wave number [19,45]. In the PWB method, the wall loss cross section σ_w is defined as $\sigma_w = P_w/S$, where P_w is the steady-state power loss caused by wall absorption, and S represents the unidirectional power density at any point inside the cavity. To arrive at an analytical expression for S, we first write the Poynting vector S_p that flows uniformly in all directions as $S_p = cW/(4\pi V)$, where W is the stored energy inside the cavity volume V. Thus, S can be calculated through the integral

$$S = \int_0^{2\pi} d\phi \int_0^{\pi/2} \cos\theta S_p \sin\theta d\theta = \frac{cW}{4V}.$$

Combined with $Q = \omega W/P_w$ (which assumes that wall loss dominates the closed cavity Q), we have

$$\sigma_w = \frac{P_w}{S} = \frac{\omega W}{Q}\frac{4V}{cW} = \frac{4kV}{Q},$$

and we finally arrive at $\alpha = \gamma \sigma_w$, where $\gamma = 1/(2\lambda^2)$.

We next conduct a sanity check of the α to σ_w relationship by creating a practical scenario. Consider a single lossy cavity with a single input port and a radiating aperture. We choose this particular scenario because it reflects the range of situations where we believe the hybrid PWB-RCM method will be relevant and valid. We calculate the radiated power from the cavity as a function of the internal loss parameter in each model, for fixed input power. In the PWB treatment, a single-mode port and an aperture are opened on the cavity with their PWB cross sections σ_{o1} and σ_{o2}, respectively. Waves are incident into the cavity through the port and exit the cavity through either the aperture or the port into a vacuum. In the RCM treatment of the same system, the port and the aperture are modeled with their corresponding radiation impedance (for the port) and radiation admittance (for the aperture).

For the study shown in Fig. 6, the dimension of the single cavity is set to $0.762 \times 0.762 \times 1.778$ m^3, which is the exact cavity dimension used in the experimental setup. The aperture radiated power P_{aper} is calculated with both treatments at 5 GHz under various cavity loss values. The aperture is set to be a circular-shaped aperture that allows approximately 75 propagating modes at 5 GHz. The results for the RCM are shown as red circles in Fig. 6. The PWB
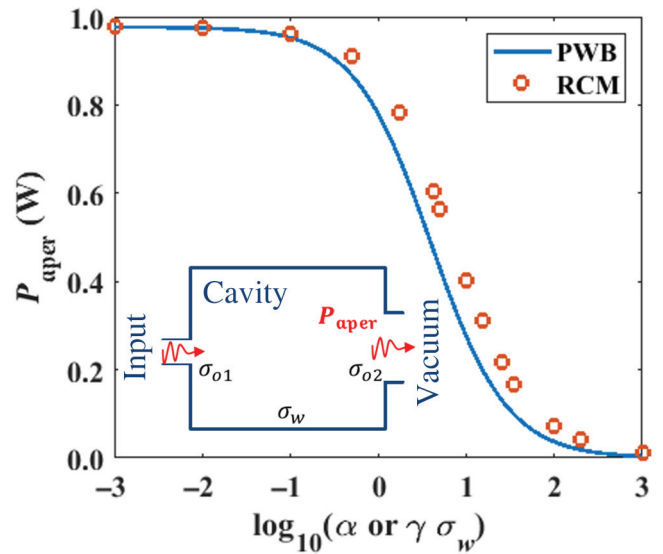

FIG. 6. The single-cavity radiated power through the aperture opening P_{aper} versus the cavity loss calculated with the PWB ($\gamma\sigma_w$) and RCM (α) methods. The input power is set as 1 W. The inset shows a schematic diagram of the single-cavity radiation setup.

results are obtained for a series of σ_w values and are shown as a blue line in Fig. 6. The factor $\gamma = 1/(2\lambda^2) = 139$ m^{-2} is applied for the PWB calculation to scale the σ_w value to α on the horizontal axis. Good agreement of aperture radiated power is found between the two models. We note that a finite discrepancy is observed in the range $\alpha \in [0.1, 100]$. This slight difference may be caused by the presence of an aperture whose dimension is comparable to the operating wavelength (the resonance regime). In this limit, the PWB formulae developed for electrically small and large apertures may require modification.

APPENDIX B: THE EXPERIMENTAL SETUP OF HYBRID MODEL LIMITATION STUDIES

As discussed in Secs. III and IV, both the PWB and RCM methods assume that the wave energy inside the subvolumes are homogeneously distributed. We would not expect the hybrid model to be effective when this assumption is violated. We experimentally test this limit of the hybrid method by creating a system with nonuniform energy distributions [see Fig. 7(a)]. In the 2-cavity cascade setup, we first cover one of the cavity walls with rf absorbing materials to create an effective "open-window" cavity. The results for the load-induced voltage statistics in this cavity can be found in Fig. 5(a). The single-cavity loss parameter is $\alpha = 25$, estimated by calculating the Q factor of the S-parameter measurements [19]. It is shown that neither the hybrid method nor the RCM method can correctly reproduce the experimental results for the load-induced voltage statistics.
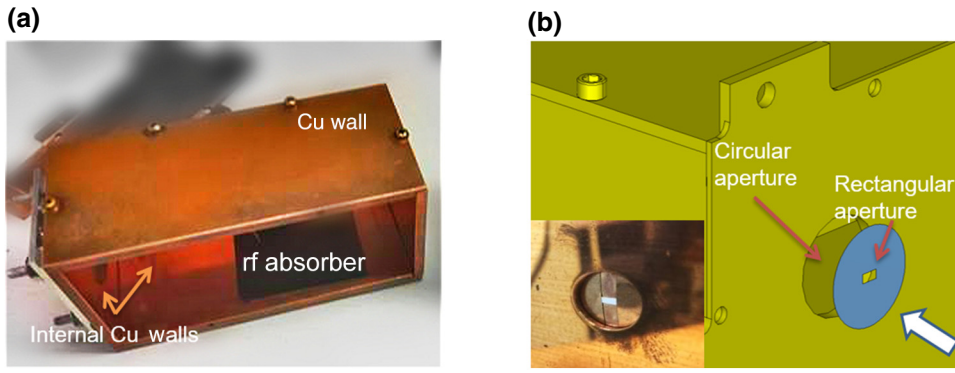
(a)

(b)

FIG. 7. (a) The open-wall view of the single cavity under extreme high-loss conditions. A piece of the rf absorber material (black rectangle) is attached at one cavity wall. (b) The schematic picture of how the rectangular-shaped aperture is created. Copper tape with a small rectangular opening (shown in blue) is placed over the original circular aperture. The inset shows a picture of the rectangular-shaped aperture.

We also test the case where the apertures are changed from a large circular-shaped aperture with approximately 100 propagating modes into a small rectangular-shaped aperture with only five propagating modes [see Fig. 7(b)]. As shown in Fig. 5(b), the hybrid model prediction deviates from the experimental results, while the full RCM prediction retains the ability to accurately predict the induced voltage PDF.

APPENDIX C: MULTICHANNEL ANALYSIS FOR THE CAVITY CASCADE SYSTEM

Within the RCM description, the nth cavity in the cavity cascade chain can be modeled by the following equation:

$$\begin{bmatrix} \underline{V}_n^i \\ \underline{V}_n^o \end{bmatrix} = \begin{bmatrix} \underline{\underline{Z}}_n^{ii} & \underline{\underline{Z}}_n^{io} \\ \underline{\underline{Z}}_n^{oi} & \underline{\underline{Z}}_n^{oo} \end{bmatrix} \begin{bmatrix} \underline{I}_n^i \\ \underline{I}_n^o \end{bmatrix}. \tag{C1}$$

The superscripts i and o refer to the input and output side of the nth cavity where we adopt the convention that "input" is on the side closest to the input TX port of the cavity chain and "output" is on the side with the RX port (see Fig. 1). The voltage vectors $\underline{V}$ and current vectors $\underline{I}$ at the input and output sides of a cavity are connected through the cavity impedance matrix, as shown in Eq. (C1). The Z matrix of the nth cavity is written as a 2×2 block matrix. Assuming that the nth cavity has m_1 and m_2 coupling channels at its input and output sides, the input vectors $(\underline{V}_n^i, \underline{I}_n^i)$ are $m_1 \times 1$, and the output vectors $(\underline{V}_n^o, \underline{I}_n^o)$ are $m_2 \times 1$. Correspondingly, the dimension of the Z matrix elements are $m_1 \times m_1, m_2 \times m_2, m_1 \times m_2$, and $m_2 \times m_1$ for $\underline{\underline{Z}}_n^{ii}, \underline{\underline{Z}}_n^{oo}, \underline{\underline{Z}}_n^{io}$, and $\underline{\underline{Z}}_n^{oi}$, respectively. For simplicity, we assume the RCM description of the off-diagonal impedance matrices as

$$\underline{\underline{Z}}_n^{oi} = (\underline{\underline{R}}_n^o)^{1/2} \underline{\underline{\xi}}_n (\underline{\underline{R}}_n^i)^{1/2}, \tag{C2}$$

and the matrices $\underline{\underline{Z}}_n^{oo,ii}$ are diagonal. The $\underline{\underline{R}}_n^{i,o}$ are the input and output radiation resistance matrices, and $\underline{\underline{\xi}}_n$ is the RCM normalized impedance matrix. Since the output side of the nth cavity is connected to the input side of the $(n+1)$th

cavity, the continuity relationships of voltages and currents between the two cavities are

$$\underline{V}_n^o = \underline{V}_{n+1}^i, \qquad \underline{I}_n^o = -\underline{I}_{n+1}^i. \tag{C3}$$

In the high-loss limit, the output current at the $(n+1)$th cavity $\underline{I}_{n+1}^o$ is much smaller than the input current at the nth cavity $\underline{I}_n^i$. By solving Eqs. (C1) and (C3) and neglecting terms $\underline{\underline{Z}}_{n+1}^{io} \underline{I}_{n+1}^o$ (small compared to the $\underline{\underline{Z}}^{ii}$ terms), the relationship between the input currents at the nth and $(n+1)$th cavities in the high-loss limit is written as

$$(\underline{\underline{Z}}_{n+1}^{ii} + \underline{\underline{Z}}_n^{oo})^{-1} \underline{\underline{Z}}_n^{oi} \underline{I}_n^i = \underline{I}_{n+1}^i.$$

We then rewrite this equation as

$$\underline{\psi}_{n+1} = \underline{\underline{\tau}}_{n \to n+1} \underline{\underline{\xi}}_n \underline{\psi}_n \tag{C4}$$

with $\quad \underline{\underline{\tau}}_{n \to n+1} = (\underline{\underline{R}}_{n+1}^i)^{1/2} (\underline{\underline{Z}}_{n+1}^{ii} + \underline{\underline{Z}}_n^{oo})^{-1} (\underline{\underline{R}}_n^o)^{1/2},$

a transition matrix that describes the coupling from the nth cavity to the $(n+1)$th cavity with $\underline{\underline{R}}_n^{i,o}$ as in (C2), and the $\underline{\psi}_n = (\underline{\underline{R}}_n^i)^{1/2} \underline{I}_n^i$ is a currentlike vector that describes the input signal of the cavity n. The power entering the nth cavity is given by

$$P_n = \frac{1}{2} \mathrm{Re}[\underline{I}_n^{i\dagger} \underline{\underline{Z}}_n^{ii} \underline{I}_n^i] = \frac{1}{2} \underline{\psi}_n^\dagger \underline{\psi}_n. \tag{C5}$$

We first assume the transition matrix $\underline{\underline{\tau}}$ to be diagonal. The input power at the $(n+1)$th cavity is written as

$$\begin{aligned} P_{n+1} &= \frac{1}{2} \underline{\psi}_{n+1}^\dagger \underline{\psi}_{n+1} \\ &= \frac{1}{2} (\underline{\underline{\tau}}_{n \to n+1} \underline{\underline{\xi}}_n \underline{\psi}_n)^\dagger (\underline{\underline{\tau}}_{n \to n+1} \underline{\underline{\xi}}_n \underline{\psi}_n) \\ &= \frac{1}{2} \sum_{i,j,k} (\psi_{n,i}^* \xi_{ji}^* |\tau_j|^2 \xi_{jk} \psi_{n,k}). \end{aligned} \tag{C6}$$

The more general cases, where the constraint of $\underline{\underline{\tau}}$ being diagonal is lifted, will be discussed later in this section.

With $\langle P_n \rangle = \frac{1}{2} \langle \underline{\psi}_n^\dagger \underline{\psi}_n \rangle$ being the average input power at the nth cavity, and the fact that $\langle \xi_{ji}^* \xi_{j'i'} \rangle = \langle \xi_{ji}^* \xi_{ji} \rangle \delta_{ii'} \delta_{jj'}$, we can further simplify Eq. (C6) as

$$\langle P_{n+1} \rangle = \langle P_n \rangle \cdot \langle |\xi|^2 \rangle \cdot \sum_j |\tau_j|^2 = \langle P_n \rangle \langle |\xi|^2 \rangle \sum_j T_j,$$

(C7)

where $T_j = |\tau_j|^2$ and the sum on j runs from all transmitting channels. Based on the relationship in Eq. (C7), we next analyze the fluctuation level of the power delivered to the load (P_L) by studying the ratio $\kappa = \langle P_L^2 \rangle / \langle P_L \rangle^2$. To simplify the following expression, $X_j = \psi_{n,j}^* \psi_{n,j}$ and $Y_j = \psi_{n+1,j}^* \psi_{n+1,j}$ are employed in the following calculations. Equation (C6) is now rewritten as $Y_j = T_j \sum_{i,i'} \psi_{n,i}^* \psi_{n,i'} \xi_{ji}^* \xi_{ji'}$, and further we have $\langle Y_j \rangle = T_j \langle |\xi|^2 \rangle \sum_i \langle X_i \rangle$. Utilizing $\langle |\xi|^4 \rangle = 2 \langle |\xi|^2 \rangle^2$ and $\langle \xi_{ji}^* \xi_{ji'} \xi_{ji}^* \xi_{ji'} \rangle = \langle \xi_{ji}^* \xi_{ji} \rangle \langle \xi_{ji'} \xi_{ji'} \rangle = 0$ when $i \neq i'$, we have

$$\sum_{jj'} \langle Y_j Y_{j'} \rangle = \langle |\xi|^2 \rangle^2 \sum_{i,i''} \langle X_i X_{i''} \rangle \left[\sum_{jj'} T_j T_{j'} + \sum_j T_j^2 \right].$$

(C8)

We then introduce a mean power transmission coefficient for the nth cavity $\bar{T}_n$ and an effective total number of channels M_n, defined as

$$\bar{T}_n = \langle |\xi|^2 \rangle \sum_j T_j, \qquad M_n^{-1} = \sum_j T_j^2 \bigg/ \left(\sum_j T_j \right)^2,$$

(C9)

respectively. Thus, we have the power transmitted into the $(n+1)$th cavity [Eq. (C7)] written as

$$\langle P_{n+1} \rangle = \bar{T}_n \langle P_n \rangle,$$

(C10)

and

$$\langle P_{n+1}^2 \rangle = \bar{T}_n^2 (1 + M_n^{-1}) \langle P_n^2 \rangle.$$

(C11)

The fluctuation level of the power after N cavities is

$$\kappa = \frac{\langle P_L^2 \rangle}{\langle P_L \rangle^2} = \frac{\langle P_1^2 \rangle}{\langle P_1 \rangle^2} \prod_{n=1}^N (1 + M_n^{-1}) = \prod_{n=1}^N (1 + M_n^{-1}).$$

(C12)

Here we utilized the fact that the power injected into the first cavity (P_1) is a fixed scalar in the case of a steady input. Since the last cavity is connected to the load with a single-mode port in the experiments, we have

$(1 + M_N^{-1}) = 2$ at the last cavity. The overall fluctuating level of the load power is

$$\kappa = \frac{\langle P_L^2 \rangle}{\langle P_L \rangle^2} = 2 \left[\prod_{n=1}^{N-1} (1 + M_n^{-1}) \right].$$

(C13)

For a system with a large number of connecting channels ($M_n \gg 1$) between the neighboring cavities, such as the circular aperture connection which allows approximately 100 propagating modes, the factor $(1 + M_n^{-1}) \to 1$. In this limit, the mean field methods are sufficient to describe the power flow for cavities with strong coupling. On the contrary, the hybrid model is not expected to work for a system with few coupling channels inside a cavity cascade. The study explains the experimental observations that hybrid models are successfully applied to systems with multimode aperture connections (see Fig. 3), while they fail to generate predictions for systems with "bottlenecks" [see Fig. 5(b)].

We also note that the proposed hybrid model assumes each input current throughout the chain is Gaussian distributed while the RCM predicts non-Gaussian statistics [17]. In the presence of a "bottleneck" connection, a deviation from Gaussian statistics of the input current distribution will be present owing to the fluctuating nature of the narrow aperture coupling.

We next expand the analysis to the more general cases where the transition matrix $\underline{\tau}$ is no longer a diagonal matrix. With Eqs. (C6) and $\overline{(C8)}$, the expression for Y_j becomes

$$Y_j = \sum_{j'j''} \tau_{jj'}^* \tau_{jj''} \sum_{i',i''} \psi_{n,i'}^* \psi_{n,i''} \xi_{j'i'}^* \xi_{j''i''}.$$

(C14)

Analogously, the average of Y_j is $\langle Y_j \rangle = \sum_{j'} \tau_{jj'}^* \tau_{jj'} \langle |\xi|^2 \rangle \sum_i \langle X_i \rangle$. With the updated $\bar{T}_n = \langle |\xi|^2 \rangle \sum_{jj'} \tau_{jj'}^* \tau_{jj'}$, we sum on j and obtain

$$\sum_j \langle Y_j \rangle = \langle |\xi|^2 \rangle \sum_{jj'} \tau_{jj'}^* \tau_{jj''} \sum_i \langle X_i \rangle = \bar{T}_n \sum_i \langle X_i \rangle,$$ (C15)

and the average of the product of the Y's is

$$\langle Y_k Y_{k'} \rangle = \sum_{j j' j'' j'''} \tau_{kj}^* \tau_{kj'} \tau_{k'j''}^* \tau_{k'j'''}$$

$$\times \sum_{i,i',i'',i'''} \langle \psi_{n,i}^* \psi_{n,i'} \psi_{n,i''}^* \psi_{n,i'''} \rangle \langle \xi_{ji}^* \xi_{j'i'} \xi_{j''i''}^* \xi_{j'''i'''} \rangle.$$

(C16)

With careful calculation, the double summation of Eq. (C16) over k and k' gives

$$
\sum_{k,k'} \langle Y_k Y_{k'} \rangle / \langle |\xi|^2 \rangle^2 = \sum_{ii'} \langle X_i X_{i'} \rangle \left[\sum_{jk} \tau_{kj}^* \tau_{kj} \right]^2
$$
$$
+ \sum_{ii'} \langle X_i X_{i'} \rangle \sum_{jj'} \left[\sum_{k} \tau_{kj}^* \tau_{kj'} \right]^2. \tag{C17}
$$

With the updated $\bar{T}_n$, we reach a similar expression of the power flow as in Eq. (C11) with the new M_n^{-1} written as

$$
M_n^{-1} = \sum_{jj'} \left[\sum_{k} \tau_{kj}^* \tau_{kj'} \right]^2 \Big/ \left[\sum_{jj'} \tau_{jj'}^* \tau_{jj'} \right]^2. \tag{C18}
$$

Thus, the conclusions of the multichannel analysis can be applied to the more general cases with the refined $\underline{\underline{\tau}}$, $\bar{T}_n$, and M_n^{-1}.

APPENDIX D: APPLYING THE HYBRID MODEL TO GENERIC CAVITY SYSTEMS

Here we propose a scheme of applying the hybrid model to more general cases, where there exists several limited-channel connections between the intermediate cavities. Because of the large power-flow fluctuations induced by these "bottlenecks," we apply RCM to better characterize these connections. A general case is shown in Fig. 8. We study the treatment of limited-channel connections between the ith and $(i + 1)$th cavities in an N-cavity cascade chain. The treatment involves four steps.

(i) Use the PWB N-cavity model to calculate the input, output power of the ith cavity $P_{\text{in}}^i|_{\text{PWB}}$, $P_{\text{out}}^i|_{\text{PWB}}$, and the input power at the last (Nth) cavity $P_{\text{in}}^N|_{\text{PWB}}$.

(ii) For the case of a bottleneck between cavity i and cavity $i + 1$ (see Fig. 8), use the calculated $P_{\text{in}}^i|_{\text{PWB}}$ and RCM treatment to calculate an ensemble of the output power of the ith cavity $P_{\text{out}}^i|_{\text{RCM}}$.

(iii) Update the input power at the last cavity by

$$
P_{\text{in}}^N|_{\text{RCM}} = P_{\text{out}}^i|_{\text{RCM}} \left. \frac{P_{\text{in}}^N}{P_{\text{out}}^i} \right|_{\text{PWB}}.
$$

Note that we therefore obtain an ensemble of the input power to the last cavity $P_{\text{in}}^N|_{\text{RCM}}$.

(iv) Use RCM to calculate an ensemble of the output power of the Nth cavity $P_{\text{out}}^N|_{\text{RCM}}$ with the ensemble of $P_{\text{in}}^N|_{\text{RCM}}$ obtained from (iii).

For cases where there exist multiple "bottlenecks" inside the chain (beyond cavity i), one may repeat procedure (ii)–(iv) by actively changing the cavity index N to the next cavity connected through a bottleneck.

APPENDIX E: HYBRID MODEL SIMPLIFICATION

Here we present a simplified treatment of the PWB-RCM hybrid method where the full-wave simulated aperture radiation admittance matrix is no longer required. We assume that all inter-cavity apertures are large, on the scale of a wavelength, i.e. the original PWB-RCM treatment is applicable. We also assume that all cavities are in the high-loss ($\alpha > 1$) limit. This Y_{aper}-free treatment will further decrease the computational cost of the hybrid model. We utilize Eqs. (C4)–(C6) to introduce the new treatment.

Consider an N-cavity cascade chain. We may treat the load connected to the output port of the Nth cavity as the $(N + 1)$th effective cavity. The induced power is equal to the input power of the $(N + 1)$th cavity:

$$
\begin{aligned}
P_{\text{load}} &= P_{N+1} \\
&= \frac{1}{2} \psi_{N+1}^{\dagger} \psi_{N+1} \\
&= \frac{1}{2} (\tau_{N\rightarrow N+1} \underline{\xi}_N \underline{\psi}_n)^{\dagger} (\tau_{N\rightarrow N+1} \underline{\xi}_N \underline{\psi}_n).
\end{aligned} \tag{E1}
$$

Here $\tau_{N\rightarrow N+1} = (R_{N+1}^i)^{1/2} (Z_{N+1}^{ii} + Z_N^{oo})^{-1} (R_N^o)^{1/2}$ is a scalar transition factor due to the fact that a single-mode port acts as a single-mode "aperture" connecting the Nth and $(N + 1)$th cavities (the load). As introduced in the main text, the radiation impedance of the port, which is used to calculate $\tau_{N\rightarrow N+1}$, is obtained from the scattering matrix measurements of the waveguide ports.

Equation (E1) is further generalized as

$$
P_{\text{load}} = \frac{1}{2} \psi_{N+1}^{\dagger} \psi_{N+1} = \frac{1}{2} |\tau_{N\rightarrow N+1}|^2 \underline{\psi}_n^{\dagger} \underline{\xi}_N^{\dagger} \underline{\xi}_N \underline{\psi}_n. \tag{E2}
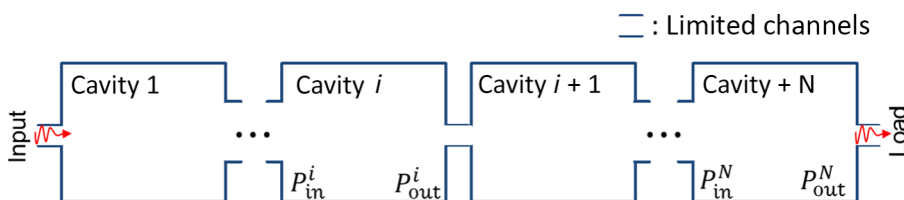$$

☐ : Limited channels

FIG. 8. Schematic of a cavity cascade array with many-channel connecting apertures between all cavities except that between cavity i and cavity $i + 1$. Note the definition of input and output powers at each cavity aperture.
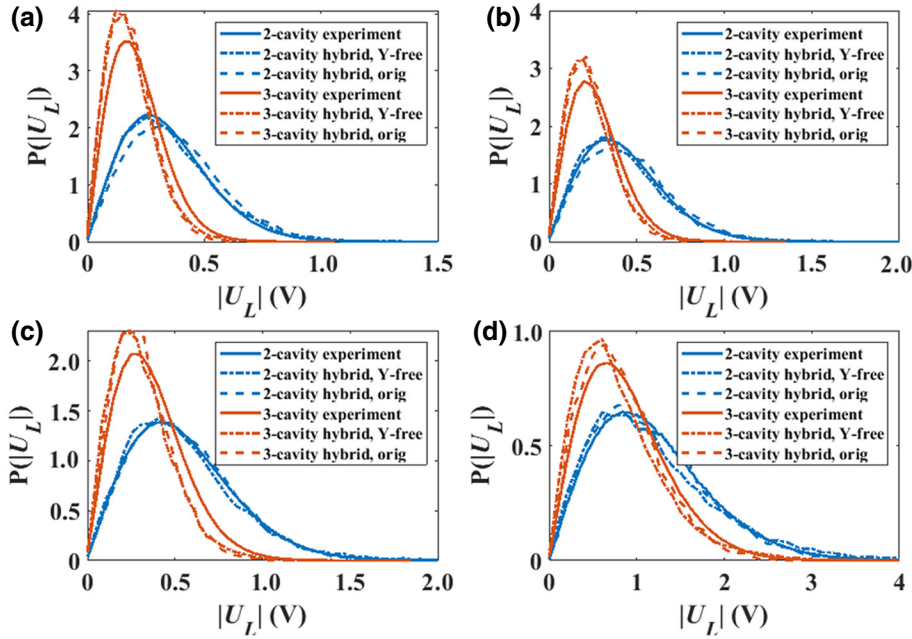
FIG. 9. The PDFs of load-induced voltage $|U_L|$ of 2- and 3-cavity experiments (solid lines), hybrid model (dashed lines), and the simplified hybrid model (dash-dotted lines). The single-cavity loss parameter is 9.7, 7.5, 5.7, and 1.7 in (a)–(d), respectively.

The ensemble average of P_{load} is

$$\langle P_{\text{load}} \rangle = \frac{1}{2}|\tau_{N\to N+1}|^2 \langle \underline{\psi}_n^\dagger \underline{\xi}_N^\dagger \underline{\xi}_N \underline{\psi}_n \rangle$$

$$= \frac{1}{2}|\tau_{N\to N+1}|^2 \underline{\psi}_n^\dagger \underline{\psi}_n \langle \underline{\xi}_N^\dagger \underline{\xi}_N \rangle. \qquad (\text{E3})$$

In the above equation, the quantity $\underline{\psi}_n$ is moved out of the ensemble averaging because only $\underline{\xi}_N$ is varying under the ensemble average, while $\underline{\psi}_n$ and $\tau_{N\to N+1}$ are not. As defined in Appendix C, we write $\underline{\psi}_n = \underline{\underline{R}}_N^{ii\,1/2} \cdot \underline{I}_n^i$ under the high-loss assumption. Here $\underline{\underline{R}}_N^{ii}$ is set as the radiation impedance of the aperture, which does not change value under ensemble averaging. The input current vector $\underline{I}_n^i$ is also considered not to change since the cavity off-diagonal impedance element $\underline{\underline{Z}}_n^{io}$ [Eq. (C1)] is small at the high-loss limit, and the input power of the Nth cavity is fixed from the prior PWB calculation. Since the input power of the Nth cavity $P_N = \frac{1}{2}\underline{\psi}_N^\dagger \underline{\psi}_N$ is given by the PWB calculation, we may further simplify Eq. (E3) as $\langle P_{\text{load}} \rangle = \frac{1}{2}|\tau_{N\to N+1}|^2 \underline{\psi}_n^\dagger \underline{\psi}_n \langle \underline{\xi}_N^\dagger \underline{\xi}_N \rangle = P_N |\tau_{N\to N+1}|^2 \cdot \langle \underline{\xi}_N^\dagger \underline{\xi}_N \rangle$. The vector element of $\underline{\xi}_N$, ξ_i, is generated using the same method as in Sec. III. The vector product $\underline{\xi}_N^\dagger \underline{\xi}_N$ is the summation of a large number of $\xi_i^* \xi_i$'s. Thus, $\underline{\xi}_N^\dagger \underline{\xi}_N$ and $\xi_i^* \xi_i$ have the same expected value according to the law of large numbers. We finally write $\langle P_{\text{load}} \rangle = P_N |\tau_{N\to N+1}|^2 \langle \xi_i^* \xi_i \rangle$ and Eq. (E2) is reduced to scalar components $P_{\text{load}} = P_N |\tau_{N\to N+1}|^2 \xi_i^* \xi_i$.

The comparison of the original hybrid model and the Y_{aper}-free hybrid model is presented in Fig. 9. Good agreement between the simplified hybrid model predictions and the experimental cases for the PDF of load-induced voltages are found. The original hybrid model slightly outperforms its simplified version for the 3-cavity cases [red curves in Figs. 9(a)–(d)], and it is expected that the accuracy of predictions will decrease for longer chains. Such an effect may be caused by the absence of an aperture admittance matrix in the simplified hybrid model. The Y_{aper}-free treatment would broaden the applicable range of the PWB-RCM hybrid method to situations where the exact shape of the aperture is unknown and the numerical simulation of the aperture is unavailable. However, this shortcut shares the same high-loss ($\alpha > 1$) assumption since it is built on the multichannel analysis (Appendix C). We also note that, for situations discussed in Appendix D, the admittance matrix of the narrow aperture (bottleneck) is required to compute the transition matrix $\underline{\underline{\tau}}$.

[1] Xin Li, Cui Meng, Yinong Liu, Edl Schamiloglu, and Sameer D. Hemmady, Experimental verification of a stochastic topology approach for high-power microwave effects, IEEE Trans. Electromagnetic Compatibility **57**, 448 (2015).

[2] Dario Fedeli, Gabriele Gradoni, Valter Mariani Primiani, and Franco Moglie, Accurate analysis of reverberation field penetration into an equipment-level enclosure, IEEE Trans. Electromagnetic Compatibility **51**, 170 (2009).

[3] B. Dietz, T. Guhr, H. L. Harney, and A. Richter, Strength Distributions and Symmetry Breaking in Coupled Microwave Billiards, Phys. Rev. Lett. **96**, 254101 (2006).

[4] J. T. Chalker and P. D. Coddington, Percolation, quantum tunnelling and the integer Hall effect, J. Phys. C: Solid State Phys. **21**, 2665 (1988).

[5] Jay D. Sau and S. Das Sarma, Realizing a robust practical Majorana chain in a quantum-dot-superconductor linear array, Nat. Commun. **3,** 964 (2012).

[6] C. W. J. Beenakker, Random-matrix theory of Majorana fermions and topological superconductors, Rev. Mod. Phys. **87,** 1037 (2015).

[7] P. Zhang and Franco Nori, Majorana bound states in a disordered quantum dot chain, New J. Phys. **18,** 043033 (2016).

[8] Matthieu Dupré, Philipp Del Hougne, Mathias Fink, Fabrice Lemoult, and Geoffroy Lerosey, Wave-Field Shaping in Cavities: Waves Trapped in a Box with Controllable Boundaries, Phys. Rev. Lett. **115,** 017701 (2015).

[9] Nadège Kaina, Matthieu Dupré, Geoffroy Lerosey, and Mathias Fink, Shaping complex microwave fields in reverberating media with binary tunable metasurfaces, Sci. Rep. **4,** 6693 (2015).

[10] Philipp del Hougne, Mohammadreza F. Imani, Timothy Sleasman, Jonah N. Gollub, Mathias Fink, Geoffroy Lerosey, and David R. Smith, Dynamic metasurface aperture as smart around-the-corner motion detector, Sci. Rep. **8,** 6536 (2018).

[11] C. Ellegaard, T. Guhr, K. Lindemann, H. Q. Lorensen, J. Nygård, and M. Oxborrow, Spectral Statistics of Acoustic Resonances in Aluminum Blocks, Phys. Rev. Lett. **75,** 1546 (1995).

[12] Gregor Tanner and Niels Søndergaard, Wave chaos in acoustics and elasticity, J. Phys. A: Math. Theor. **40,** R443 (2007).

[13] Yves Aurégan and Vincent Pagneux, Acoustic scattering in duct with a chaotic cavity, Acta Acust. United Acust. **102,** 869 (2016).

[14] E. Doron, U. Smilansky, and A. Frenkel, Experimental Demonstration of Chaotic Scattering of Microwaves, Phys. Rev. Lett. **65,** 3072 (1990).

[15] Paul So, Steven M. Anlage, Edward Ott, and Robert N. Oerter, Wave Chaos Experiments with and Without Time Reversal Symmetry: GUE and GOE Statistics, Phys. Rev. Lett. **74,** 2662 (1995).

[16] U. Kuhl, M. Martínez-Mares, R. A. Méndez-Sánchez, and H.-J. Stöckmann, Direct Processes in Chaotic Microwave Cavities in the Presence of Absorption, Phys. Rev. Lett. **94,** 144101 (2005).

[17] Gabriele Gradoni, Thomas M. Antonsen, and Edward Ott, Impedance and power fluctuations in linear chains of coupled wave chaotic cavities, Phys. Rev. E **86,** 046204 (2012).

[18] Luigi Gagliardi, Davide Micheli, Gabriele Gradoni, Franco Moglie, and Valter Mariani Primiani, Coupling between multipath environments through a large aperture, IEEE Antennas Wirel. Propag. Lett. **14,** 1463 (2015).

[19] Bo Xiao, Thomas M. Antonsen, Edward Ott, Zachary B. Drikas, Jesus Gil Gil, and Steven M. Anlage, Revealing underlying universal wave fluctuations in a scaled ray-chaotic cavity with remote injection, Phys. Rev. E **97,** 062220 (2018).

[20] S. Ma, B. Xiao, R. Hong, B. D. Addissie, Z. B. Drikas, T. M. Antonsen, E. Ott, and S. M. Anlage, Classification and prediction of wave chaotic systems with machine learning techniques, Acta Phys. Pol. A **136,** 757 (2019).

[21] Gregor Tanner, Klaus Richter, and Jan-Michael Rost, The theory of two-electron atoms: Between ground state and complete fragmentation, Rev. Mod. Phys. **72,** 497 (2000).

[22] R. U. Haq, A. Pandey, and O. Bohigas, Fluctuation Properties of Nuclear Energy Levels: Do Theory and Experiment Agree? Phys. Rev. Lett. **48,** 1086 (1982).

[23] Y. Alhassid, The statistical theory of quantum dots, Rev. Mod. Phys. **72,** 895 (2000).

[24] Jean Philippe Parmantier, Numerical coupling models for complex systems and results, IEEE Trans. Electromagnetic Compatibility **46,** 359 (2004).

[25] Sameer Hemmady, Thomas M. Antonsen, Edward Ott, and Steven M. Anlage, Statistical prediction and measurement of induced voltages on components within complicated enclosures: A wave-chaotic approach, IEEE Trans. Electromagnetic Compatibility **54,** 758 (2012).

[26] Carl E. Baum, Tom K. Liu, and Fred M. Tesche, On the analysis of general multiconductor transmission-line networks, Interaction Note **350,** 467 (1978).

[27] D. A. Hill, M. T. Ma, A. R. Ondrejka, B. F. Riddle, M. L. Crawford, and R. T. Johnk, Aperture excitation of electrically large, lossy cavities, IEEE Trans. Electromagnetic Compatibility **36,** 169 (1994).

[28] D. A. Hill, Plane wave integral representation for fields in reverberation chambers, IEEE Trans. Electromagnetic Compatibility **40,** 209 (1998).

[29] Isabelle Junqua, Jean-Philippe Parmantier, and François Issac, A network formulation of the power balance method for high-frequency coupling, Electromagnetics **25,** 603 (2005).

[30] Gregory B. Tait, Robert E. Richardson, Michael B. Slocum, Michael O. Hatfield, and Manuel J. Rodriguez, Reverberant microwave propagation in coupled complex cavities, IEEE Trans. Electromagnetic Compatibility **53,** 229 (2011).

[31] Louis Kovalevsky, Robin S. Langley, Philippe Besnier, and Jerome Sol, in *2016 ESA Workshop on Aerospace EMC (Aerospace EMC)* (IEEE, Valencia, Spain, 2016), p. 1.

[32] J. W. McKown and R. L. Hamilton, Ray tracing as a design tool for radio networks, IEEE Netw. **5,** 27 (1991).

[33] Lauri Savioja and U. Peter Svensson, Overview of geometrical room acoustic modeling techniques, J. Acoust. Soc. Am. **138,** 708 (2015).

[34] Janis Bajars, David J. Chappell, Niels Søndergaard, and Gregor Tanner, Transport of phase space densities through tetrahedral meshes using discrete flow mapping, J. Comput. Phys. **328,** 95 (2017).

[35] Janis Bajars, David J. Chappell, Timo Hartmann, and Gregor Tanner, Improved approximation of phase-space densities on triangulated domains using discrete flow mapping with p-refinement, J. Sci. Comput. **72,** 1290 (2017).

[36] Timo Hartmann, Satoshi Morita, Gregor Tanner, and David J. Chappell, High-frequency structure- and air-borne sound transmission for a tractor model using dynamical energy analysis, Wave Motion **87,** 132 (2019).

[37] Sameer Hemmady, Xing Zheng, Edward Ott, Thomas M. Antonsen, and Steven M. Anlage, Universal Impedance Fluctuations in Wave Chaotic Systems, Phys. Rev. Lett. **94,** 014102 (2005).

[38] Xing Zheng, Thomas M. Antonsen, and Edward Ott, Statistics of impedance and scattering matrices of chaotic

microwave cavities with multiple ports, Electromagnetics **26**, 37 (2006).

[39] Xing Zheng, Thomas M. Antonsen, and Edward Ott, Statistics of impedance and scattering matrices in chaotic microwave cavities: Single channel case, Electromagnetics **26**, 3 (2006).

[40] Xing Zheng, Sameer Hemmady, Thomas M. Antonsen, Steven M. Anlage, and Edward Ott, Characterization of fluctuations of impedance and scattering matrices in wave chaotic scattering, Phys. Rev. E **73**, 046208 (2006).

[41] G. Casati, F. Valz-Gris, and I. Guarnieri, On the connection between quantization of nonintegrable systems and statistical theory of spectra, Lettere al Nuovo Cimento **28**, 279 (1980).

[42] O. Bohigas, M. J. Giannoni, and C. Schmit, Characterization of Chaotic Quantum Spectra and Universality of Level Fluctuation Laws, Phys. Rev. Lett. **52**, 1 (1984).

[43] J. A. Hart, T. M. Antonsen, and E. Ott, Effect of short ray trajectories on the scattering statistics of wave chaotic systems, Phys. Rev. E **80**, 041109 (2009).

[44] Jen-Hao Yeh, James A. Hart, Elliott Bradshaw, Thomas M. Antonsen, Edward Ott, and Steven M. Anlage, Experimental examination of the effect of short ray trajectories in two-port wave-chaotic scattering systems, Phys. Rev. E **82**, 041114 (2010).

[45] Gabriele Gradoni, Jen-Hao Yeh, Bo Xiao, Thomas M. Antonsen, Steven M. Anlage, and Edward Ott, Predicting the statistics of wave transport through chaotic cavities by the random coupling model: A review and recent progress, Wave Motion **51**, 606 (2014).

[46] Bo Xiao, Thomas M. Antonsen, Edward Ott, and Steven M. Anlage, Focusing waves at arbitrary locations in a ray-chaotic enclosure using time-reversed synthetic sonas, Phys. Rev. E **93**, 052205 (2016).

[47] Shukai Ma, Bo Xiao, Zachary Drikas, Bisrat Addissie, Ronald Hong, Thomas M. Antonsen, Edward Ott, and Steven M. Anlage, Wave scattering properties of multiple weakly coupled complex systems, Phys. Rev. E **101**, 022201 (2020).

[48] Min Zhou, Edward Ott, Thomas M. Antonsen, and Steven M. Anlage, Nonlinear wave chaos: Statistics of second harmonic fields, Chaos **27**, 103114 (2017).

[49] Min Zhou, Edward Ott, Thomas M. Antonsen, and Steven M. Anlage, Scattering statistics in nonlinear wave chaotic systems, Chaos: Interdiscip. J. Nonlinear Sci. **29**, 033113 (2019).

[50] Gabriele Gradoni, Thomas M. Antonsen, Steven M. Anlage, and Edward Ott, A statistical model for the excitation of cavities through apertures, IEEE Trans. Electromagnetic Compatibility **57**, 1049 (2015).

[51] Magnus Hoijer and Lars Kroon, Field statistics in nested reverberation chambers, IEEE Trans. Electromagnetic Compatibility **55**, 1328 (2013).

[52] R. Serra, A. C. Marvin, F. Moglie, V. Mariani Primiani, A. Cozza, L. R. Arnaut, Y. Huang, M. O. Hatfield, M. Klingler, and F. Leferink, Reverberation chambers a la carte: An overview of the different mode-stirring techniques, IEEE Electromagnetic Compatibility Mag. **6**, 63 (2017).

[53] Matthew Frazier, Biniyam Taddese, Thomas Antonsen, and Steven M. Anlage, Nonlinear Time Reversal in a Wave Chaotic System, Phys. Rev. Lett. **110**, 063902 (2013).

[54] Matthew Frazier, Biniyam Taddese, Bo Xiao, Thomas Antonsen, Edward Ott, and Steven M. Anlage, Nonlinear time reversal of classical waves: Experiment and model, Phys. Rev. E **88**, 062910 (2013).

[55] Sameer Hemmady, Xing Zheng, James Hart, Thomas M. Antonsen, Edward Ott, and Steven M. Anlage, Universal properties of two-port scattering, impedance, and admittance matrices of wave-chaotic systems, Phys. Rev. E **74**, 036213 (2006).

[56] Zachary B. Drikas, Jesus Gil Gil, Sun K. Hong, Tim D. Andreadis, Jen-Hao Yeh, Biniyam T. Taddese, and Steven M. Anlage, Application of the random coupling model to electromagnetic statistics in complex enclosures, IEEE Trans. Electromagnetic Compatibility **56**, 1480 (2014).

[57] M. V. Berry, Regularity and chaos in classical mechanics, illustrated by three deformations of a circular 'billiard', Eur. J. Phys. **2**, 91 (1981).

[58] Y. V. Fyodorov and D. V. Savin, Statistics of impedance, local density of states, and reflection in quantum chaotic systems with absorption, J. Exp. Theor. Phys. Lett. **80**, 725 (2004).

[59] A. Rehemanjiang, M. Allgaier, C. H. Joyner, S. Müller, M. Sieber, U. Kuhl, and H.-J. Stöckmann, Microwave Realization of the Gaussian Symplectic Ensemble, Phys. Rev. Lett. **117**, 064101 (2016).

[60] Don Coppersmith and Shmuel Winograd, Matrix multiplication via arithmetic progressions, J. Symb. Comput. **9**, 251 (1990).

[61] Ronny Gunnarsson and Mats Backstrom, in *2014 International Symposium on Electromagnetic Compatibility* (IEEE, Gothenburg, Sweden, 2014), p. 169. http://iee explore.ieee.org/document/6930897/

[62] Jesus Gil Gil, Zachary B. Drikas, Tim D. Andreadis, and Steven M. Anlage, Prediction of induced voltages on ports in complex, three-dimensional enclosures with apertures, using the random coupling model, IEEE Trans. Electromagnetic Compatibility **58**, 1535 (2016).

[63] Jen-Hao Yeh, Thomas M. Antonsen, Edward Ott, and Steven M. Anlage, First-principles model of time-dependent variations in transmission through a fluctuating scattering environment, Phys. Rev. E **85**, 015202 (2012).

[64] J.-H. Yeh, Z. Drikas, J. Gil Gil, S. Hong, B. T. Taddese, E. Ott, T. M. Antonsen, T. Andreadis, and S. M. Anlage, Impedance and scattering variance ratios of complicated wave scattering systems in the low loss regime, Acta Phys. Pol. A **124**, 1045 (2013).

[65] T. Hartmann, S. Morita, G. Tanner, and D. J. Chappell, High-frequency structure- and air-borne sound transmission for a tractor model using dynamical energy analysis, Wave Motion **87**, 132 (2019).

[66] Jiexiong Yan, John F. Dawson, Andy C. Marvin, Ian David Flintoft, and Martin P. Robinson, 3-D diffusion models for predicting reverberant electromagnetic power density in loaded enclosures, IEEE Trans. Electromagnetic Compatibility **61**, 1362 (2019).

[67] Dong Ho Wu, Jesse S. A. Bridgewater, Ali Gokirmak, and Steven M. Anlage, Probability Amplitude Fluctuations in Experimental Wave Chaotic Eigenmodes with and Without Time-Reversal Symmetry, Phys. Rev. Lett. **81**, 2890 (1998).

[68] Adnan Farasartul, Valon Blakaj, Sendy Phang, Thomas M. Antonsen, Stephen C. Creagh, Gabriele Gradoni, and Gregor Tanner, Wireless power distributions in multi-cavity systems at high frequencies. Proc. R. Soc. A (to be published).

[69] Jen-Hao Yeh and Steven M. Anlage, In situ broadband cryogenic calibration for two-port superconducting microwave resonators, Rev. Sci. Instrum. **84**, 034706 (2013).

[70] Shen Lin, Zhen Peng, Edl Schamiloglu, Zachary B. Drikas, and Thomas Antonsen, in *2019 IEEE International Symposium on Electromagnetic Compatibility, Signal & Power Integrity (EMC+SIPI)* (IEEE, New Orleans, 2019), p. 499. https://ieeexplore.ieee.org/document/8825194/